MATERIALS FORUM VOLUME 31 - 2007
Edited by J.M. Cairney and S.P. Ringer

DEVELOPMENT OF A LOW MELTING POINT WHITE CAST IRON FOR USE IN COMPOSITE ALLOY MANUFACTURE

P. Huggett[1], B. Ben-Nissan[2]

[1] Materials Solutions Pty Ltd, 16 Ferntree Close, Thornlie, WA 6108, Australia
[2] Department of Chemistry, Materials and Forensic Sciences, PO BOX 123 Broadway, NSW 2007, Australia

ABSTRACT

White cast irons are used extensively throughout the mining industry for their wear resistant properties. Since their original development in the early 1900's researchers have continued to develop a range of white cast iron compositions with varying degrees of hardness, toughness or corrosion resistance. This study focuses on the development of a low melting point white cast iron which has applications in the composite alloy manufacturing industry. The compositional range for the study was developed through analysis of the iron-chromium-carbon phase diagram. Experimental work has included the casting and thermal analysis of a range of alloy compositions. The microstructures of the alloys have been studied to determine the relationship with the phase diagram, and a comparison of the experimental data with computer generated phase diagrams is presented. The results of this study permitted an alloy white cast iron to be produced with a melting point of approximately 1200°C. The experimentally derived thermal data for the liquidus and solidus temperatures are generally lower compared to the predicted data based on CALPHAD simulations.

1. INTRODUCTION

Recently a new process has been developed [1-3] which permits composites of steel and white cast iron to be produced using a vacuum heat treatment process. During the heat treat treatment cycle, the white iron is heated until the temperature reaches typically 50°C above the liquidus temperature of the white cast iron.

Before the development of a new vacuum heat treatment process for bonding steel to white cast iron could be started, it was necessary to consider the raw materials and in particular the melting point (or liquidus) of the white cast iron.

Common modern vacuum heat treatment furnaces typically have an upper temperature limit of 1200 to 1300°C. Commercial white cast irons normally have a liquidus temperature above 1290°C. Examples of commercial white cast iron liquidus temperatures are provided in Table 1.

In order to allow standard vacuum heat treatment equipment to be used for the development of the bonding process, it was therefore necessary to develop a lower melting point white cast iron, preferably with a liquidus temperature of around 1200°C.

2. WHITE CAST IRON METALLURGY

Cast irons are heterogeneous ferrous alloys, which solidify with a eutectic phase. They contain iron, carbon and silicon as the major alloying elements and often incorporate chromium, nickel, manganese, molybdenum, copper and other elements to enhance specific chemical and mechanical properties.

Table 1. Typical liquidus temperatures for commercial white cast irons

Alloy Designation[4]	Description	Liquidus (°C)
Cr 27	Eutectic High Chromium White Cast Iron	1296
CrMo 15 3	Hypoeutectic Chromium – Molybdenum White Cast Iron	1246
Cr 35	Hypereutectic High Chromium White Cast Iron	1440

The iron-chromium-carbon alloy system used for this study typically exhibits three main microstructural types depending on the nature of the proeutectic phase. These are a hypoeutectic, eutectic and hypereutectic alloy. The phases present for each of these types of alloys are essentially the same, consisting of a hard carbide and a softer ferrous structure, only differing in the nature of the proeutectic phase formed.

Chromium is the major alloying element used in white irons in addition to iron and carbon. Chromium is a strong carbide former, and can form a variety of carbides depending on the overall composition and carbon level.

The following carbide types can be typically found in chromium white irons:

i. M_7C_3 where M usually consists of chromium and iron.
ii. M_3C where M is usually iron (cementite).
iii. M_2C where M is usually molybdenum.
iv. $M_{23}C_3$ where M is usually chromium and iron, and occurs when the chromium/carbon ratio is high.

More than one element may combine with the carbon to form the hard carbides, and typically iron is present along with the chromium, creating a complex carbide $(Fe,Cr)_7C_3$. Elements such as vanadium and niobium can also be used as alloying elements, creating more complex carbides.

3. IRON-CHROMIUM-CARBON PHASE DIAGRAM

A large systematic study of the iron-rich corner of the Fe-Cr-C system was conducted by Bungardt et al [5]. Subsequent studies by Jackson [6], and Thorpe and Chicco [7] have resulted in more accurate representations of the system. For the purpose of this study, the liquidus projection used comes from the work conducted by Thorpe and Chicco, and is shown in Figure 1.

Based on the liquidus projection represented in Figure 1, four proeutectic or primary phases can occur on solidification depending on the composition of the alloy:

a) austenite (gamma Fe)
b) ferrite (alpha delta Fe)
c) M_7C_3 carbide
d) M_3C carbide

The invariant liquidus reactions that are shown in the liquidus projection (Figure 1) are summarised in Table 2:

Table 2. Summary of invariant reactions

U1 : L + alpha delta Fe -> gamma Fe + M_7C_3
U2 : L + M_7C_3 -> gamma Fe + M_3C
P1 : L + alpha delta Fe -> gamma Fe
e1 : L -> gamma Fe + Fe_3C

The reaction sequence for the Fe-Cr-C metastable system based on the study by Thorpe and Chicco is shown in Figure 2.

Study of the Fe-Cr-C phase diagram shows the eutectic trough follows a reducing temperature as it approaches the U2 triple point. At a composition of approximately 4 wt% carbon and 10% chromium, the liquidus temperature is estimated to be 1200°C.

This composition is not considered practical from a commercial manufacturing perspective, and the effect of adding silicon, manganese and other minor alloying elements needs to be considered.

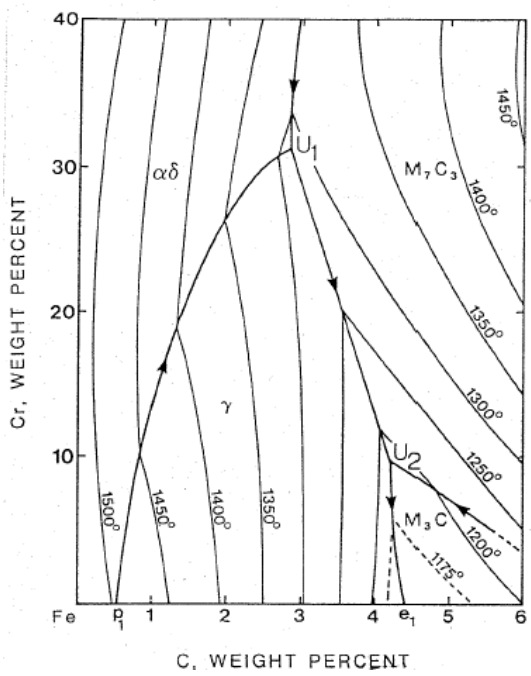

Figure 1. Liquidus projection for the Fe-Cr-C System [7].

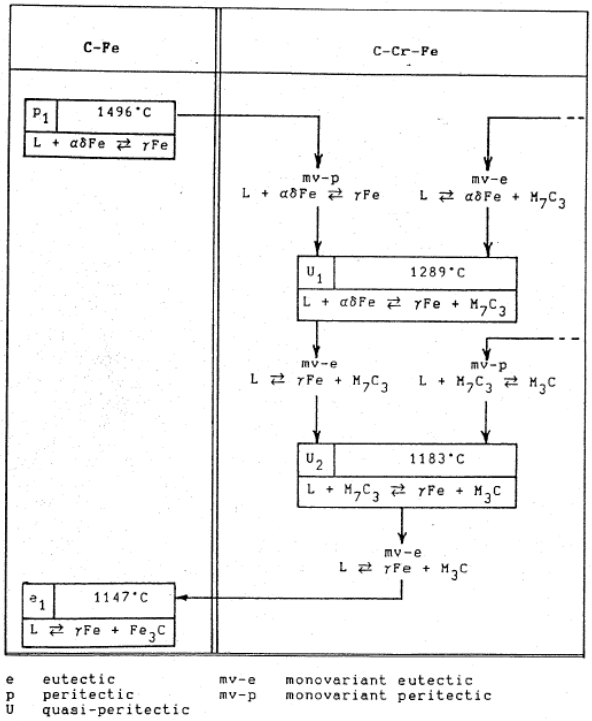

Figure 2. Summary of Reaction Sequences for the Fe-Cr-C System [7].

In recent years computer aided phase diagrams (CALPHAD) have become a popular tool for studying the effects of alloy composition variations. Commercial computer software programs such as Thermocalc [8] allow a range of compositions to be studied, and isopleths to be established. These computer aided calculations can then be compared with actual thermal analysis data from production melts to provide a comparison of accuracy.

In a study conducted by Schon and Sinatora [9] on the simulation of solidification paths for the Fe-Si-Cr-C alloy system, a range of computer predicted microstructures were compared to experimentally observed microstructures. The experimental results obtained from the Schon and Sinatora study showed close correlation between the predicted and the observed microstructures. In particular the target composition for this study of Fe-12Cr-4C would be expected to have a microstructure of M_7C_3 eutectic carbide, with M_3C carbide surrounding M_7C_3 carbide particles, and ledeburite. The M_3C carbides surrounding the M_7C_3 carbide particles was a result of the quasi-peritectic reaction U2 observed in Thorpe and Chico's data [7] and shown in Figure 2.

In a separate study by Du and Morral [10], a prediction was made for the lowest melting point eutectic in the Fe-Cr-Mo-V-C alloy system. Du and Morral's data showed small variations in liquidus temperatures between the predicted and the experimental data. Gomez-Acebo *et al* [11] presented a further study on the low melting point eutectics in the Fe-Cr-Mn-Mo-C alloy system.

Figure 3 represents the predicted phase diagram for the Fe-30Cr-C alloy series. This phase diagram was calculated using the Thermocalc [8] software package.

The predicted phase diagram for the Fe-10Cr-C alloy series which was suggested earlier from the Fe-Cr-C liquidus projection has a low melting point close to 1200°C. The eutectic point from the Fe-10Cr-C alloy series has a predicted value close to the experimental data determined by Thorpe and Chico [7].

Commercial alloys normally contain approximately 0.5 weight percent silicon, and nominally 1.0 weight percent manganese. The target alloy microstructure for a balanced combination of toughness and wear resistance should contain a high proportion of retained austenite with a high carbide volume fraction. Increasing the manganese content and adding nickel to the alloy will provide an increased proportion of retained austenite in the as-cast microstructure.

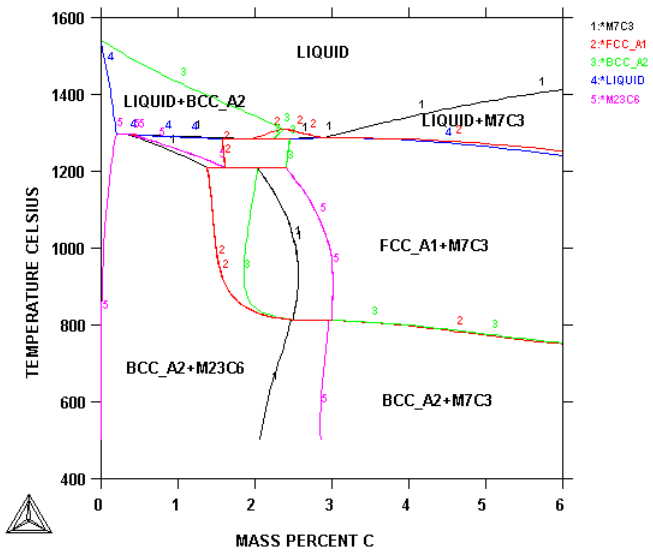

Figure 3. Calculated Phase Diagram for the Fe-30Cr-C Alloy Series [8]

If the chromium content drops too low beyond the 10 to 12 weight percent chromium level towards the U2 triple point (refer Figure 1), the carbide formed will be a combination of M_7C_3 with some M_3C. The M_3C carbide has a lower hardness compared to the M_7C_3 carbide and will potentially reduce the wear performance of the low melting point alloy. To overcome the potential for the formation of M_3C carbide, the chromium content should be increased to approximately 12 weight percent. The predicted phase diagram for the Fe-12Cr-C alloy system is shown in Figure 4.

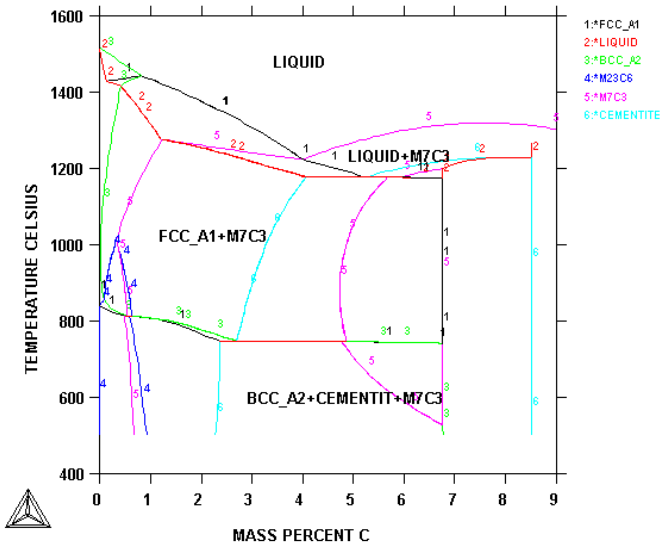

Figure 4. Calculated Phase Diagram for Fe-12Cr-C Alloy Series [8]

Figure 4 suggests the target alloy composition of Fe-12Cr-4C should have a liquidus temperature of approximately 1200°C.

The potential effect for addition of silicon, manganese and nickel to the Fe-12Cr-C alloy system predicted phase diagram is shown in Figure 5 (based on Thermocalc). Note the addition of the silicon, manganese and nickel has increased the predicted liquidus temperature to approximately 1230°C. The eutectic carbon content has also slightly reduced to approximately 3.6 to 3.7 weight percent.

Figure 5 also suggests the presence of a quasi-peritectic reaction of:

$$Liquid + M_7C_3 \rightarrow M_7C_3 + M_3C(Cementite)$$

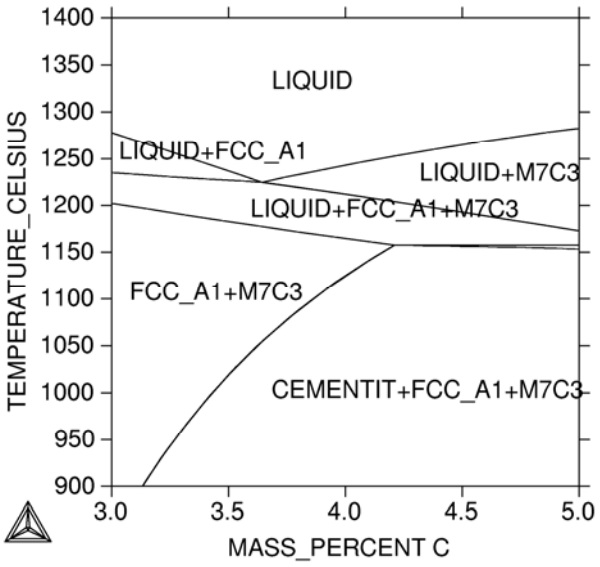

Figure 5. Calculated Phase Diagram for the Fe-12Cr-1.0Ni-0.6Si-1.6Mn-C Alloy Series [8]

The review of past work conducted on the Fe-Cr-C phase diagram suggests an alloy having the nominal composition of Fe-12Cr-1.0Ni-0.6Si-1.6Mn-4.0C will exhibit a eutectic microstructure consisting of M_7C_3 eutectic carbide, with M_3C carbide surrounding M_7C_3 carbide particles, with austenite and ledeburite. The estimated liquidus temperature for this alloy is 1200°C. The computer generated phase diagrams predict a higher eutectic temperature of approximately 1230°C.

4. EXPERIMENTAL

The experimental development of the low melting point alloy involved the systematic melting and casting of a range of alloy compositions and incorporating analytical measurements including thermal analysis, chemical analysis and metallography.

The range of alloy compositions studied is summarised in Table 3.

Each alloy composition (charge) was produced from commercial foundry grade raw materials including ferrochrome, ferrosilicon, electrolytic manganese, nickel pellets, steel scrap and graphite. The charge was then melted in an Inductotherm 75kW, 50kg pop-up induction melting furnace using clay graphite crucibles and heated to a temperature of 1500°C.

Thermal analysis recording for each alloy charge was performed using the commercially available MeltLab thermal analysis system, which records the cooling temperature of the insulated cup at 1 second intervals. The setup for the thermal analysis is shown diagrammatically in Figure 6.

At the completion of the thermal analysis, each sample was sectioned and polished to check and review the microstructure, and collated against the thermal cooling curve. The thermal cooling curves were then analysed to determine the thermal arrests representing the liquidus and solidus reactions.

Table 3. Summary of Test Alloy Compositions

Alloy	Element Composition (weight %)					
	Cr	C	Si	Mn	Ni	Fe
A1	8.0	3.4	0.5	2.0	0.0	Bal
A2	8.0	3.6	0.5	2.0	0.0	Bal
A3	8.0	3.9	0.5	2.0	0.0	Bal
A4	8.0	4.2	0.5	2.0	0.0	Bal
B1	10.0	3.3	0.5	1.6	1.0	Bal
B2	10.0	3.6	0.5	1.6	1.0	Bal
B3	10.0	4.1	0.5	1.6	1.0	Bal
C1	12.0	4.1	0.6	1.6	1.0	Bal

5. RESULTS AND DISCUSSION

The alloy compositions that make up the group of trial alloys from the range shown in Table 3 are shown relative to the published data from Thorpe and Chico [7] in Figure 7.

The proximity of the Fe-8Cr-2Mn-0.5Si-C series to the M_3C phase boundary suggests these alloys will form predominantly M_3C carbides during solidification. Based on the position of the Fe-10Cr-2Mn-0.5Si-4.1C alloy to the liquidus projection, it would be expected this alloy to be essentially eutectic in nature. The Fe-12Cr-1.6Mn-1.0Ni-0.5Si-4.1C alloy is also shown overlaying the eutectic trough for the liquidus projection.

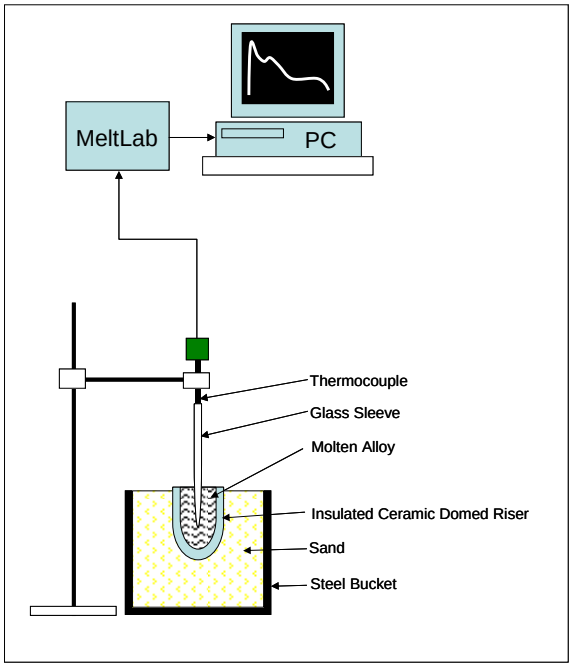

Figure 6. Schematic Diagram for Thermal Analysis Setup

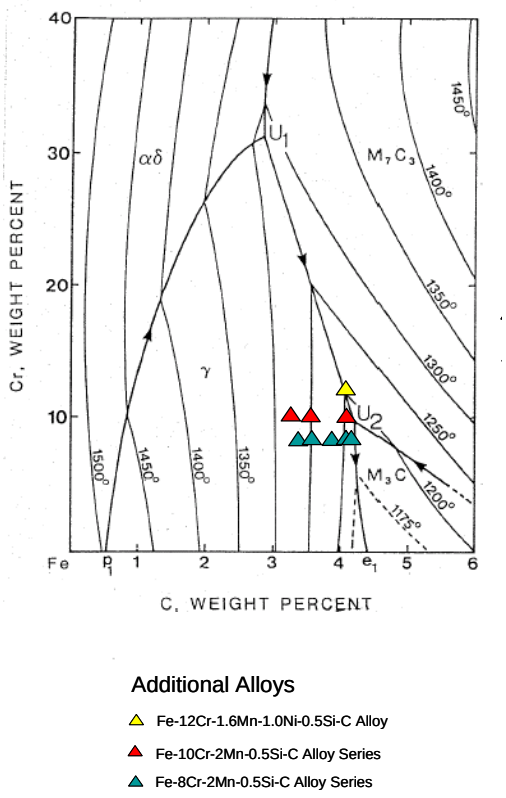

Figure 7. Relationship of Trial Alloy Compositions to Fe-Cr-C Phase Diagram (by Thorpe and Chico [33])

Each of the alloy melts produced in the induction furnace exhibited excellent melting characteristics with minimal slag development, high fluidity and clean, oxide free metal. Pouring of the alloy melts was highly compatible with standard high chromium white irons, with minimal dross and inclusions. The liquid melt surface exhibited low oxide formation and exhibited high flow movement under power from the induction furnace. Overall all of the trial alloys exhibited favorable characteristics for foundry applications.

The microstructures for the test alloys are summarised in Table 4. The microstructure for the final low melting point alloy (Alloy C1) is shown in Figure 8. The microstructure consists of eutectic M_7C_3 carbides with some M_3C carbide covering the M_7C_3 carbides as a result of the quasi-peritectic reaction, and a ferrous matrix of ledeburite with retained austenite.

Table 4. Summary of Alloy Microstructures

Alloy	Microstructure
A1	Primary austenite with partial transformation to ledeburite, and eutectic M_7C_3 with substantial M_3C covering the M_7C_3 carbides
A2	Primary austenite with partial transformation to ledeburite, and eutectic M_7C_3 with substantial M_3C covering the M_7C_3 carbides
A3	Primary austenite with partial transformation to ledeburite, and eutectic M_7C_3 with substantial M_3C covering the M_7C_3 carbides
A4	Primary austenite with partial transformation to ledeburite, and eutectic M_7C_3 with substantial M_3C covering the M_7C_3 carbides
B1	Primary austenite with partial transformation to ledeburite, and eutectic M_7C_3 with M_3C covering M_7C_3 particles
B2	Primary austenite with partial transformation to ledeburite, and eutectic M_7C_3 with M_3C covering M_7C_3 particles
B3	Primary austenite with partial transformation to ledeburite, and eutectic M_7C_3 with M_3C covering M_7C_3 particles
C1	M_7C_3 eutectic, M_3C covering M_7C_3 particles, ledeburite and retained austenite

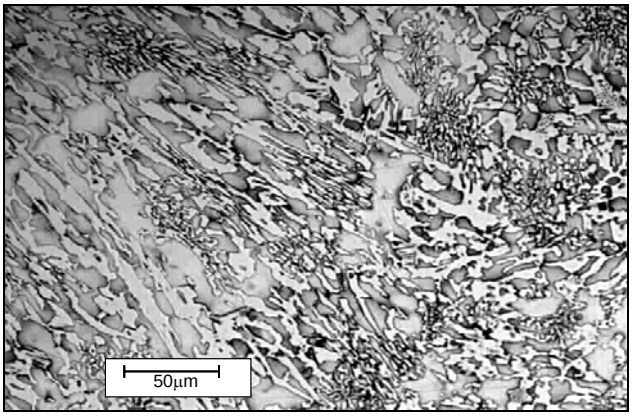

Figure 8. Typical microstructure for the Fe-12Cr-1.6Mn-1.0Ni-0.5Si-4.1C (Alloy C1) Low Melting Point White Cast Iron (Etched in Acid-Ferric Chloride)

The initial alloy series produced was the Fe-8Cr-2Mn-0.5Si-C series. The liquidus temperatures were not considered low enough to satisfy the requirements for the vacuum heat treatment phase of the study, and the presence of the high volume fraction of M_3C carbide would potentially reduce the abrasive wear performance of the alloy.

The chromium in the alloy was increased to 10 weight percent and the "B" alloy series showed improved liquidus temperature data, and a higher volume fraction of M_7C_3 carbides, however there was still further room for lowering the liquidus temperature and avoiding the detrimental M_3C carbides. It was possible that the presence of manganese may have been acting as a chromium substitute in the alloy. Based on the previous studies on element distribution, nickel partitions slightly less to the carbides compared to manganese, and therefore providing a greater austenite stabilising benefit to the ferrous matrix.

The final target alloy of Fe-12Cr-1.6Mn-1.0Ni-0.5Si-4.1C successfully resulted in a low liquidus temperature and a high volume fraction of retained M_7C_3 carbide. The addition of nickel has suppressed the transformation of the austenite to ledeburite at moderate cooling rates.

The typical thermal analysis cooling curve for the experimental alloys is shown in Figure 9. The thermal arrests observed from the thermal analysis cooling curves for all of the experimental alloys are summarised in Table 5. The liquidus and solidus for the Fe-8Cr-2.0Mn-0.5Si-C alloy series are summarised in the form of an experimental phase diagram in Figure 10 and compared to the CALPHAD predicted phase diagrams in Figure 11.

Table 5. Measured Thermal Arrests for Trial Alloys

Alloy	Liquidus (°C)	Solidus (°C)
A1	1271	1185
A2	1265	1184
A3	1226	1179
A4	1247	1181
B1	1277	1201
B2	1272	1200
B3	1257	1197
C1	1209	1194

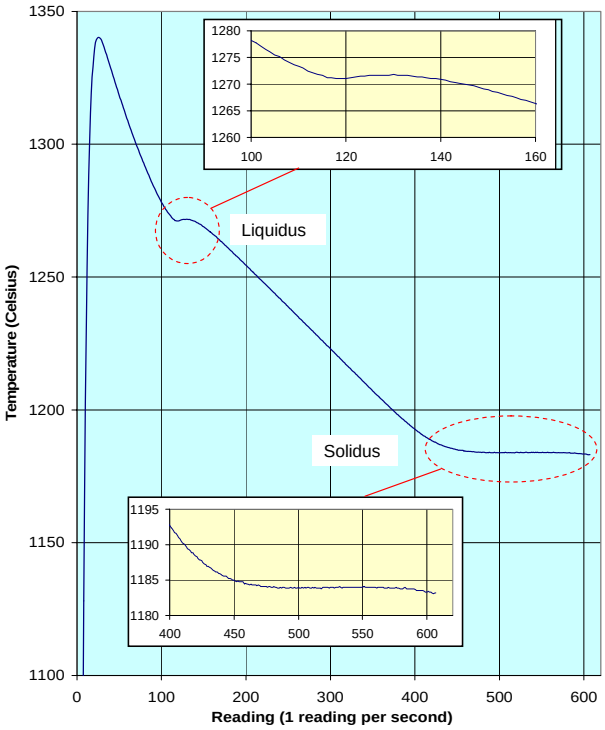

Figure 9. Typical Thermal Analysis Cooling Curve for Fe-8.0Cr-2.0Mn-0.5Si-3.4C Alloy

There is generally a close agreement between the experimental data obtained through this study and the published and predicted phase diagrams. In both the "A" and "B" series of experimental data there appears to be errors with the measured liquidus temperatures, and this could be the result of possible chemical composition differences, particularly the addition of manganese and silicon to the experimental melts.

Significantly the proposed low melting point alloy having the composition Fe-12Cr-1.6Mn-1.0Ni-0.5Si-4.1C exhibits a near eutectic composition, which is also confirmed by the fine carbide structure shown in the microstructure (refer Figure 8).

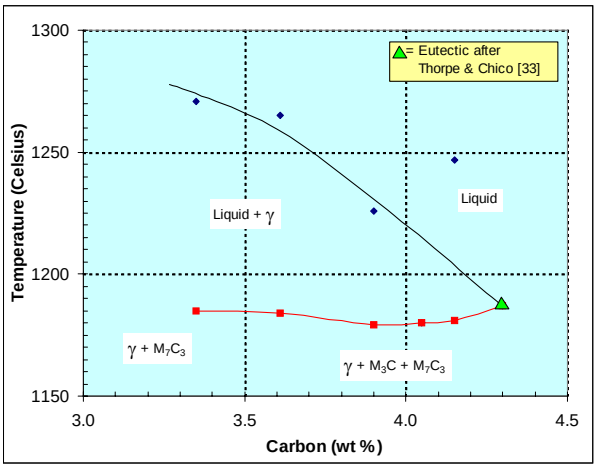

Figure 10. Phase Diagram Based on Experimental Data for Fe-8Cr-2Mn-0.5Si-C Alloy Series with Published Data from Thorpe and Chico

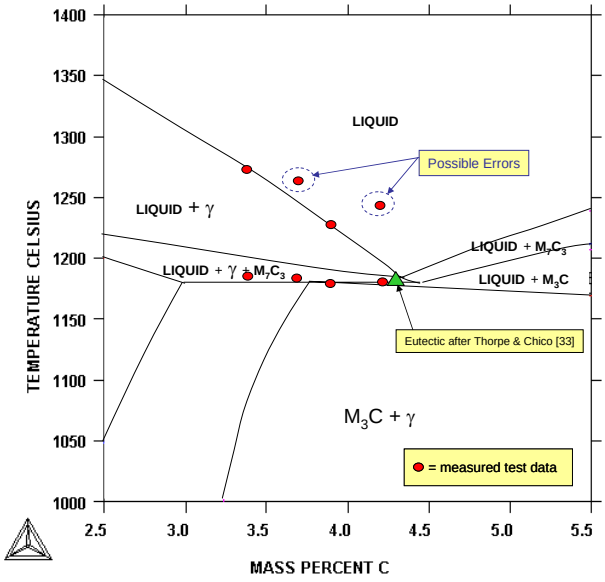

Figure 11. Comparison of Experimental Data for Fe-8Cr-2Mn-0.5Si-C Alloy Series with Predicted Data from Thermocalc

Errors were observed with the experimental data collected from this study, and this could be the result of either:

i. Chemical composition variations
ii. Non-equilibrium cooling conditions
iii. Variations in starting pouring temperature
iv. Variations in positioning of thermocouple

The thermal analysis data obtained from this study represents a practical application of thermal measurement for foundry applications and is fully representative of the cooling rates and alloy conditions experienced within a foundry. The data is therefore applicable when considering transfer of the technology to pilot scale and full scale production trials.

6. CONCLUSION

The experimental work outlined in this study has permitted the development of a low melting point white iron having the nominal composition of:

Carbon	=	4.1 weight %
Chromium	=	12.0 weight %
Manganese	=	1.6 weight %
Nickel	=	1.0 weight %
Silicon	=	0.5 weight %
Iron	=	Balance

The liquidus temperature for the alloy was measured as 1209^{o}C, and the solidus temperature was measured as 1194^{o}C.

The measured thermal arrests are in close agreement with published thermal data for the Fe-Cr-C phase diagram. The measured thermal arrests are lower compared to predicted thermal data from CALPHAD software results.

The microstructure of the low melting point alloy consists of a small volume fraction of primary austenite, with a eutectic of M_7C_3 carbides and austenite. Some of the M_7C_3 carbides have undergone a quasi-peritectic reaction which has been previously observed.. The austenite has undergone a partial transformation to form ledeburite (ferrite plus M_3C carbide in the form of cementite).

The thermal analysis data developed from this study is in close agreement with previously published data for the Fe-Cr-C alloy system. The experimental data varies from the CALPHD predicted data, and there were some errors observed with the experimental data that suggested possible chemical composition variations, thermocouple position variations or potential non-equilibrium cooling conditions within the alloy melts.

The data presented in this study for the development of the low melting point alloy has been obtained from pilot scale foundry production using typical melting and casting methods of larger foundry applications. The data is therefore typical of practical foundry practice. The measured thermal data, observed microstructures and alloy compositions are all achievable using standard foundry equipment.

References

1. P.G. Huggett, R. Wuhrer, B. Ben-Nissan and K. Moran, *Proc. 3rd Int. Conf. Adv. Mat. Processing*, 2005, pp83-88
2. P. Huggett, R. Wuhrer, B. Ben-Nissan and K. Moran, *Materials Forum*, 2006, Vol 30, pp23-29.
3. Australian Patent AU2001277412 B2
4. AS2027-2007, Standards Australia, 2007
5. K. Bungardt, E. Kunze and E. Horne, *Arch. Eisenhuttenwes*., 1958, Vol. 29, pp 193-203.
6. R.S. Jackson, *Jour of the Iron and Steel Institute*, 1970, pp 163-167.
7. W.R. Thorpe & B. Chico, *Metallurgical Transactions*, 1985, Vol. 16A, pp 1541-1549.
8. Thermo-Calc TCW3 Software, 2005, Foundation of Computational Thermodynamics, Stockholm, Sweden.
9. C.G. Schon and A. Sinatora, *CALPHAD*, 1998, Vol 22, pp437-448.
10. H. Du and J. E. Morral, *Jour. of Alloys and Compounds*, 1997, Vol 247, pp122-127.
11. T. Gomez-Acebo, M. Sarasola and F. Castro, *CALPHAD*, 2003, Vol 27, pp325-334.